Electronic Supplementary Information (ESI)

Nanoconfinement-induced Calcium ion Redox Charge Storage of V_2CT_x MXene

Suman Yadav and Narendra Kurra*

Department of Chemistry, Indian Institute of Technology Hyderabad, Kandi-502284, Sangareddy, Telangana State, India.

*Corresponding Author
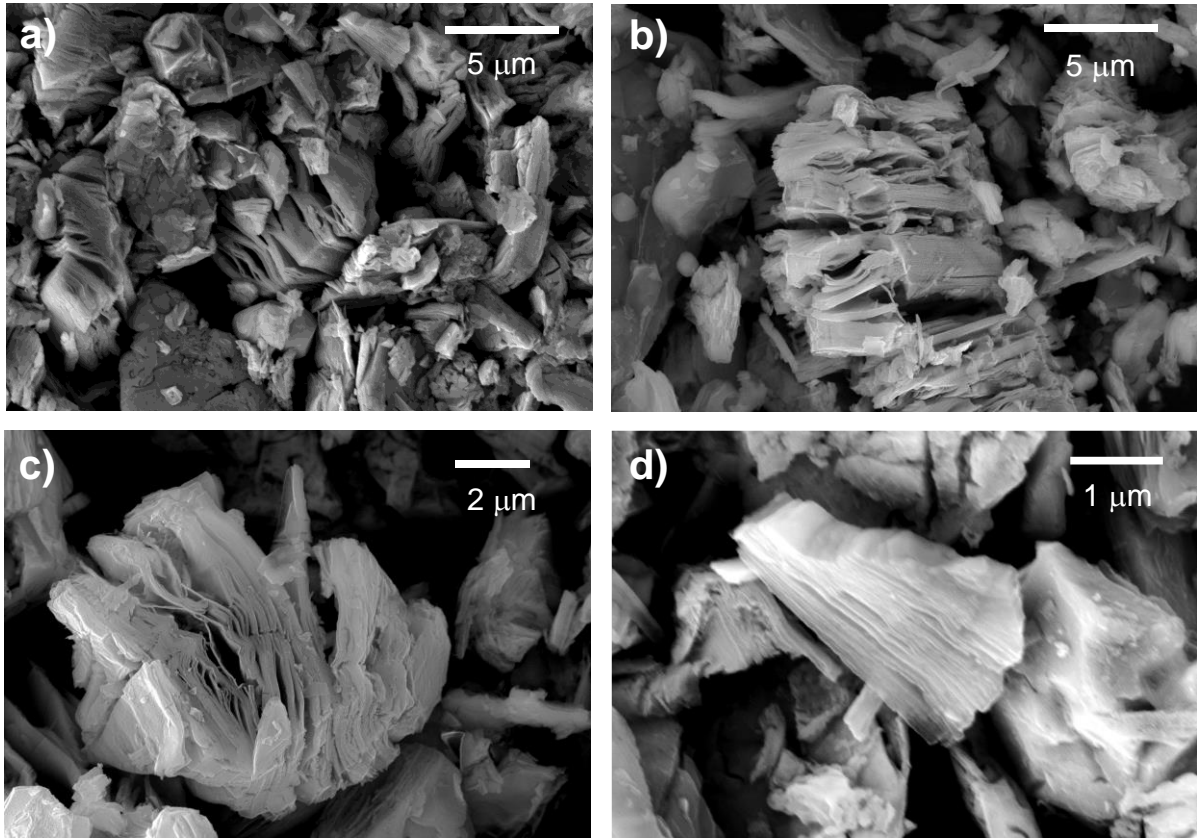
E-mail: narendra@chy.iith.ac.in

Fig. S1 SEM images of *ml*-V$_2$CT$_x$ MXene at low (a,b) and high (c,d) magnifications.

Fig. S1 shows the open and accordion-like morphology for *ml*-V$_2$CT$_x$ at different magnifications. Alhabeb *et al.* compared the HF concentration (30 wt%, 10 wt%, and 5 wt%) for the removal of the 'Al' atomic layer from the Ti$_3$AlC$_2$ MAX phase and hence concluded that the 5 wt% HF is sufficient for the etching of Al atomic layer from the MAX precursor.[1] However, the accordion-like morphology of *ml*-Ti$_3$C$_2$T$_x$ for 5 wt% etchant is not as prevalent as 30 wt% (as per as SEM imaging is concerned). Mixed acid etchant (HF/HCl) was used for the synthesis of *ml*-V$_2$CT$_x$ MXene.[2] The concentrated HF etchant may introduce a high density of defects in V$_2$CT$_x$ MXene when compared to a mixed acid etchant (HF/HCl) with a lower content of HF. The enlargement of the *d*-spacing of 5.5 Å (2θ ~ 7.34˚, corresponding to a *d*-spacing of 12.03 Å) for the *ml*-V$_2$CT$_x$ in comparison with the parent MAX phase is clear evidence of etching of 'Al' atomic layers.
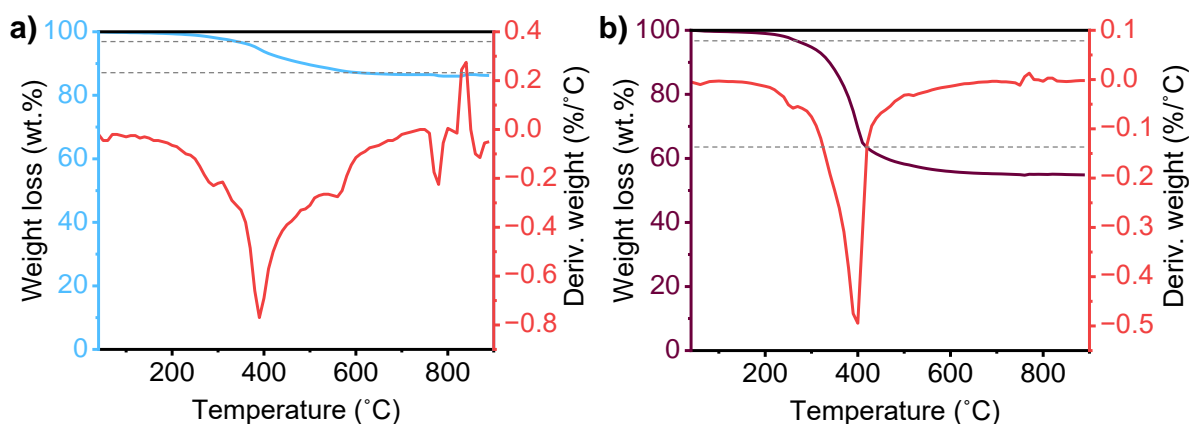
Fig. S2 Thermogravimetric curves with the derivative of weight loss of (a) *ml*-V$_2$CT$_x$ MXene powder (blue) and (b) pre-intercalated *ml*-V$_2$CT$_x$ MXene powder (vinous).

To further characterize the adsorption/intercalation of EMIM-TFSI ionic liquid into *ml*-V$_2$CT$_x$ MXene, thermogravimetric analysis was done for *ml*-V$_2$CT$_x$ MXene powder (blue) (Fig. S2a) and pre-intercalated *ml*-V$_2$CT$_x$ MXene powder (vinous) (Fig. S2b). The characteristic decomposition at a temperature of 400 °C is attributed to the EMIM-TFSI, which is not the case for the pristine *ml*-V$_2$CT$_x$ MXene (Fig. S2a). In pristine *ml*-V$_2$CT$_x$ MXene, the weight loss (up to 10 wt%) at high temperatures (>350 °C) is attributed to the dissociation of surface functional groups and also chemisorbed or structural water removal from multilayer powder.[2] However, in the case of the pre-intercalated *ml*-V$_2$CT$_x$ MXene sample, significant weight loss of up to 40 wt% is due to the decomposition of EMIM-TFSI besides the residual structural water desorption and functional groups decomposition.[3] The total weight loss is 30 wt% for the decomposition of EMIM-TFSI ionic liquid. Due to the non-volatile nature and low vapor pressure of EMIM-TFSI, the typical incorporation of ionic liquid is estimated to be 30 w/w% into V$_2$CT$_x$.
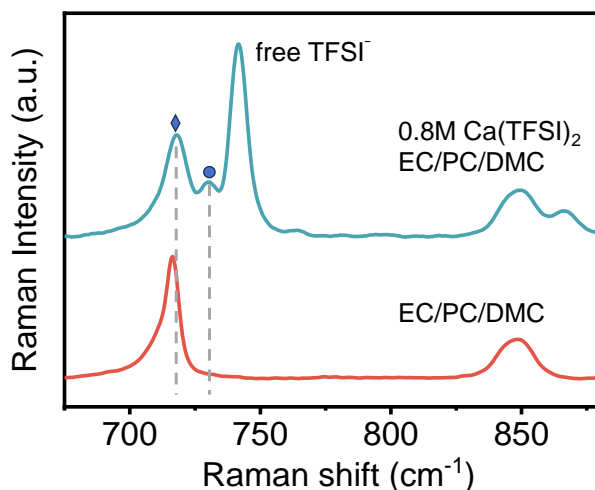
Fig. S3 Raman spectra of pure solvent (EC/PC/DMC) (red) and 0.8M Ca(TFSI)$_2$ /EC/PC/DMC electrolyte (blue), ◆ -- pure solvent, ● -- Ca-ion coordinated solvent.

In Raman spectra of 0.8M Ca(TFSI)$_2$/EC/PC/DMC electrolyte, the peak at 718 cm^{-1} corresponds to the solvent mixture (i.e., EC/PC/DMC); however, two additional peaks at 730 cm^{-1} and 741 cm^{-1} correspond to the coordination of Ca-ions with the EC/PC/DMC. The sharp peak at 741 cm^{-1} corresponds to a free TFSI anion in the electrolyte. The characteristic Raman signatures of the electrolyte at a concentration of 0.8M Ca(TFSI)$_2$/EC/PC/DMC are in accordance with the reported literature.[4]
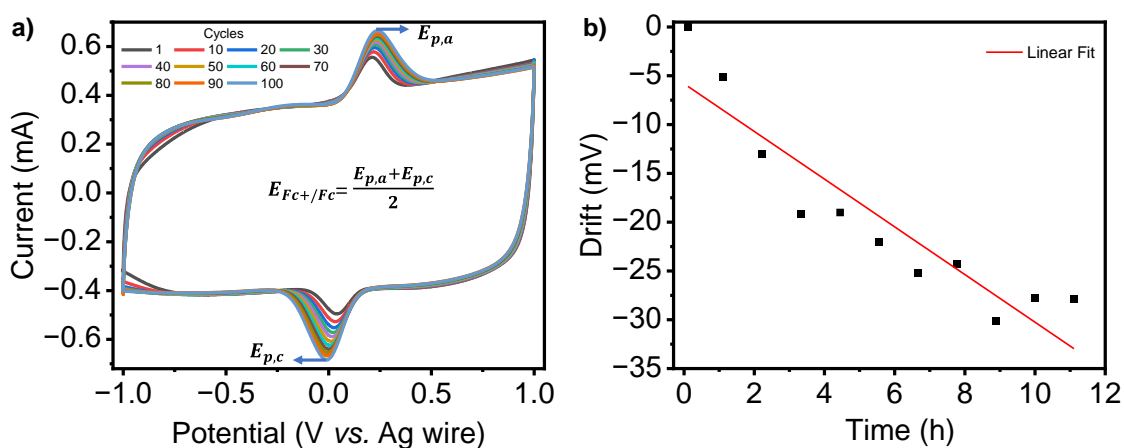

Fig. S4 (a) Cyclic voltammograms of a 3-electrode cell consisting of a mixture of 15 mM ferrocene + 0.8 M Ca(TFSI)$_2$/EC/PC/DMC electrolyte at a scan rate of 10 mV s^{-1}. (b) drift of the Ag wire reference electrode over 11 hours in electrolyte mixture.

Fig. S4 shows the 3-electrode data of Fc$^+$/Fc redox couple with the drift in the potential of the Ag wire over 11 hours. The half-wave potential of the ferrocenium/ferrocene redox couple is given by

$$E_{Fc+/Fc} = \frac{E_{p,a} + E_{p,c}}{2}$$

where $E_{Fc+/Fc}$ is the reduction potential of the ferrocenium/ferrocene redox couple, $E_{p,a}$ and $E_{p,c}$ are anodic and cathodic peak potentials, respectively. The potential of the Fc$^+$/Fc redox couple is 0.12 V *vs.* Ag wire, and it is 0.4 V *vs.* SHE.[5] Hence the potential of the Ag wire is 0.27 V *vs.* SHE.
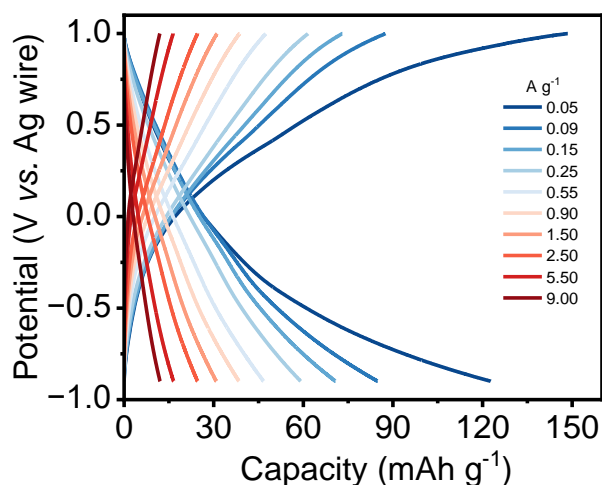

Fig. S5 The galvanostatic charge-discharge profiles at different current densities (0.05, 0.09, 0.15, 0.25, 0.55, 0.90, 1.50, 2.50, 5.50, and 9.0 A g^{-1}).
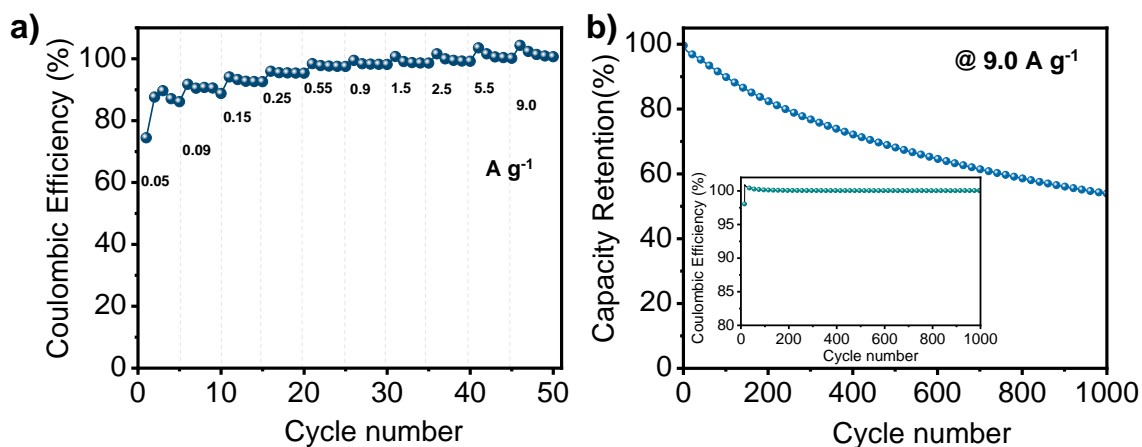
Fig. S6 Electrochemical performance of pre-intercalated *ml*-V$_2$CT$_x$ MXene in 0.8M Ca(TFSI)$_2$/EC/PC/DMC electrolyte. (a) Coulombic efficiency versus cycle number plot at different current densities (0.05, 0.09, 0.15, 0.25, 0.55, 0.90, 1.50, 2.50, 5.50, and 9.0 A g^{-1}). (b) Cycling performance of pre-intercalated *ml*-V$_2$CT$_x$ MXene electrode in non-aqueous 0.8M Ca(TFSI)$_2$ electrolyte over 1000 cycles (capacity retention of ~54%) at a current density of 9.0 A g^{-1} and inset showing the Coulombic efficiency with cycle number.

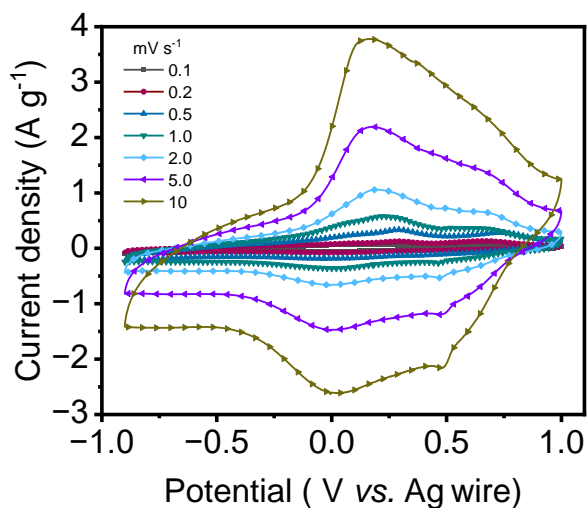**Fig. S7** (a) Cyclic voltammograms of pre-intercalated *ml*-V$_2$CT$_x$ MXene in 0.8M Ca(TFSI)$_2$/EC/PC/DMC electrolyte at various scan rates (0.1, 0.2, 0.5, 1.0, 2.0, 5.0, 10 mV s^{-1}).
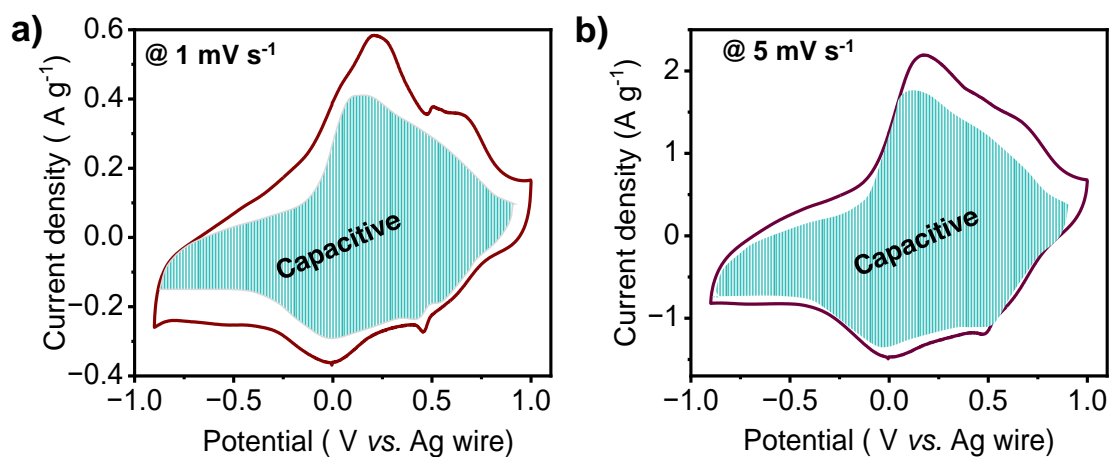
Fig. S8 CV curves of pre-intercalated *ml*-V$_2$CT$_x$ MXene at (a) 1 mV s^{-1} and (b) 5 mV s^{-1} scan rates, shaded regions correspond to capacitive contributions (green), that are estimated based on k_1k_2 analysis.
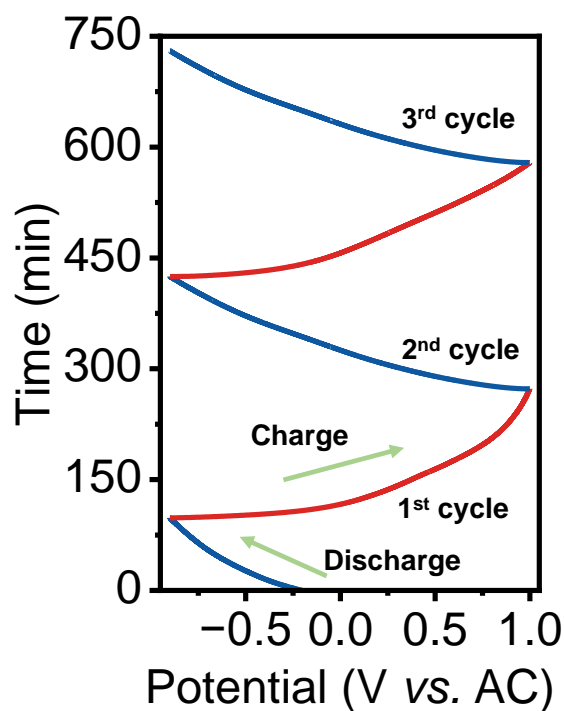

Fig. S9 Galvanostatic charge-discharge (GCD) profiles of pre-intercalated *ml*-V$_2$CT$_x$ MXene in 0.8M Ca(TFSI)$_2$ /EC/PC/DMC during *in-situ* XRD measurements.
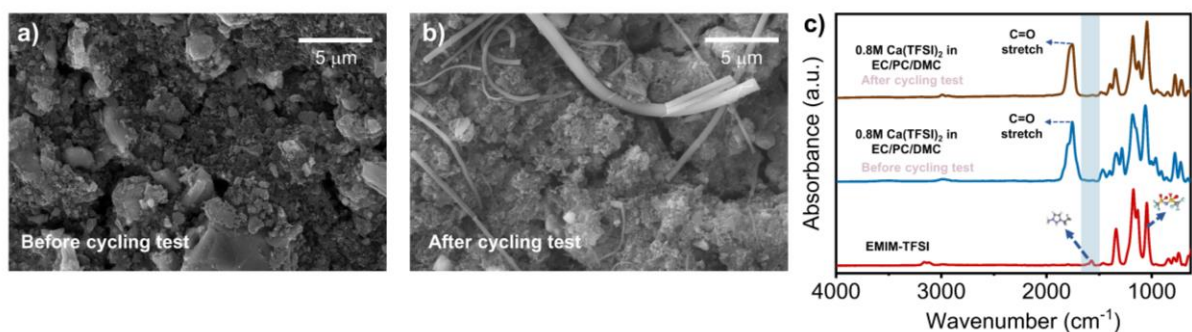
Fig. S10 Top view SEM images of pre-intercalated *ml*-V$_2$CT$_x$ MXene (a) before and (b) after cycling the electrode. (c) Attenuated total reflectance (ATR) - FTIR spectra of pure EMIM-TFSI ionic liquid (red) and 0.8M Ca(TFSI)$_2$/EC/PC/DMC electrolyte before (blue) and after (brown) 100 charge/discharge cycles.

As shown in Fig. S10c, the EMIM$^+$ peak at 1574 cm^{-1} (C=C stretching) is hardly noticed in the electrolyte before and after cycling (highlighted). There is a sharp absorbance peak at 1048 cm^{-1} (C-F stretching) corresponding to TFSI$^-$ is present in both neat ionic liquid (reference sample) and cycled electrolyte (TFSI signature peak is from Ca(TFSI)$_2$). However, the intense peak at 1763 cm^{-1} observed in both before and after electrolyte cycling is due to the C=O stretching in cyclic and linear carbonate-based solvents.
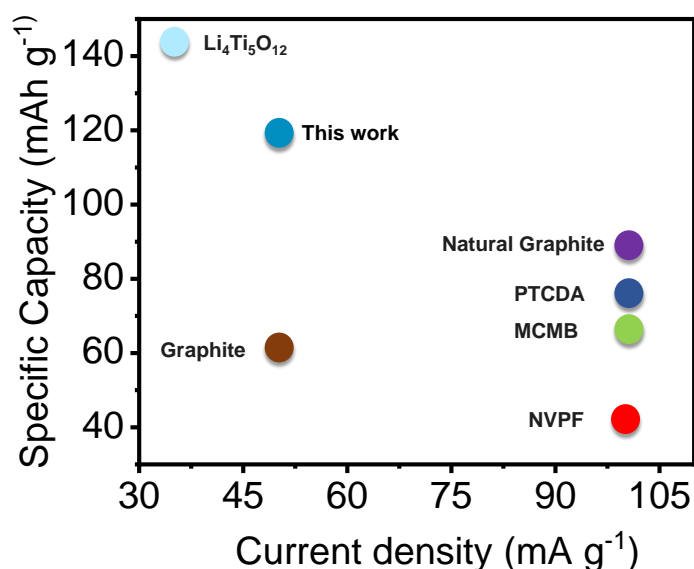

Fig. S11 Comparison of specific calciation capacities of different reported electrode materials with that of pre-intercalated *ml*-V$_2$CT$_x$ MXene (This work).

Table S1: Comparison of electrochemical performances of different electrode materials for electrochemical storage of Ca-ions.

S. No.	Working electrode	Electrolyte	Reversible capacity (mAh g^{-1}) @ Current density (A g^{-1})/C-rate	Cycle number/ capacity retention	Potential window	References
1.	NVPF	1M Ca(PF$_6$)$_2$ in EC/PC	87 @ 0.01	500/90%	-1 – 1.5 V vs AC	**6**
2.	PEDOT-V$_2$O$_5$	1M Ca(ClO$_4$)$_2$ in Acetonitrile /Water	157.2 @ 1	7000/90.8%	-0.6 – 1.2 V vs Ag/AgCl	**7**
3.	PTCDA	3.5 m Ca(FSI)$_2$ in EC/PC/DMC/EMC	75.4 @ 0.1	350/84.7%	0.5 – 3 V vs AC	**8**
4.	MCMB (artificial graphite)	0.7 M Ca(PF$_6$)$_2$ in EC:DMC:EMC	66 @2C	300/94%	3 – 5.3 V	**9**
5.	Graphite	1 m Ca(TFSI)$_2$ in tetraglyme	62 @ 0.05	no capacity decay during 2000 cycles	-1.0 – 1.0 V vs SHE	**10**
6.	Natural graphite	0.5 m (Ca(BH$_4$)$_2$ in dimethylacetamide	87 @ 0.1	200/negligible degradation	0.2 – 1.5 V vs Ca/Ca^{2+}	**11**

Abbreviation: NVPF- Sodium- vanadium fluorophosphate (Na$_{1.5}$VPO$_{4.8}$F$_{0.7}$), Ca(PF$_6$)$_2$- Calcium hexafluorophosphate, PEDOT - Poly 3,4-ethylenedioxythiophene, Ca(ClO$_4$)$_2$- Calcium perchlorate, PTCDA- 3,4,9,10-perylenetetracarboxylicdianhydride, Ca(FSI)$_2$- Calcium bis(fluorosulfonyl)imide, MCMB- mesocarbon microbead, Ca(TFSI)$_2$- Calcium(II) Bis(trifluoromethanesulfonyl)imide, Ca(BH$_4$)$_2$- Calcium borohydride.

REFERENCES

1.   M. Alhabeb, K. Maleski, B. Anasori, P. Lelyukh, L. Clark, S. Sin and Y. Gogotsi, *Chem. Mater.*, 2017, **29**, 7633-7644.

2.   K. Matthews, T. Zhang, C. E. Shuck, A. VahidMohammadi and Y. Gogotsi, *Chem. Mater.*, 2022, **34**, 499-509.

3.   M. Seredych, C. E. Shuck, D. Pinto, M. Alhabeb, E. Precetti, G. Deysher, B. Anasori, N. Kurra and Y. Gogotsi, *Chem. Mater.*, 2019, **31**, 3324-3332.

4.   J. D. Forero-Saboya, E. Marchante, R. B. Araujo, D. Monti, P. Johansson and A. Ponrouch, *J. Phys. Chem. C*, 2019, **123**, 29524-29532.

5.   J. M. Shellhamer, P. A. Chando, S. Pathreeker, X. Wang and I. D. Hosein, *J. Phys. Chem. C*, 2023, **127**, 19900-19905.

6.   Z.-L. Xu, J. Park, J. Wang, H. Moon, G. Yoon, J. Lim, Y.-J. Ko, S.-P. Cho, S.-Y. Lee and K. Kang, *Nat. Commun.*, 2021, **12**, 3369.

7.   X. Hao, L. Zheng, S. Hu, Y. Wu, G. Zhang, B. Li, M. Yang and C. Han, *Mater. Today Energy*, 2023, **38**, 101456.

8.   J. Li, C. Han, X. Ou and Y. Tang, *Angew. Chem. Int. Ed.*, 2022, **61**, e202116668.

9.   S. Wu, F. Zhang and Y. Tang, *Adv. Sci.*, 2018, **5**, 1701082.

10. S. J. Richard Prabakar, A. B. Ikhe, W. B. Park, K.-C. Chung, H. Park, K.-J. Kim, D. Ahn, J. S. Kwak, K.-S. Sohn and M. Pyo, *Adv. Sci.*, 2019, **6**, 1902129.

11. J. Park, Z.-L. Xu, G. Yoon, S. K. Park, J. Wang, H. Hyun, H. Park, J. Lim, Y.-J. Ko, Y. S. Yun and K. Kang, *Adv. Mater.*, 2020, **32**, 1904411.